Inorganic Chemistry

Article

pubs.acs.org/IC

Popular C_{82} Fullerene Cage Encapsulating a Divalent Metal Ion Sm^{2+}: Structure and Electrochemistry

Ziqi Hu,[†] Yajuan Hao,[‡] Zdeněk Slanina,[§] Zhenggen Gu,[‡] Zujin Shi,*[,†] Filip Uhlík,[∥] Yunfeng Zhao,[‡] and Lai Feng*[,‡]

[†]Beijing National Laboratory for Molecular Sciences, State Key Lab of Rare Earth Materials Chemistry and Applications, College of Chemistry and Molecular Engineering, Peking University, Beijing 100871, China

[‡]College of Physics, Optoelectronics and Energy & Collaborative Innovation Center of Suzhou Nano Science and Technology, Soochow University, Suzhou 215006, China

[§]Life Science Center of Tsukuba Advanced Research Alliance, University of Tsukuba, Tsukuba 305-8577, Japan

[∥]Department of Physical and Macromolecular Chemistry, Faculty of Science, Charles University in Prague, Albertov 6, 128 43 Praha 2, Czech Republic

Supporting Information

ABSTRACT: Two $Sm@C_{82}$ isomers have been well characterized for the first time by means of ^{13}C NMR spectroscopy, and their structures were unambiguously determined as $Sm@C_{2v}(9)$-C_{82} and $Sm@C_{3v}(7)$-C_{82}, respectively. A combined study of single crystal X-ray diffraction and theoretical calculations suggest that in $Sm@C_{2v}(9)$-C_{82} the preferred Sm^{2+} ion position shall be located in a region slightly off the C_2 axis of $C_{2v}(9)$-C_{82}. Moreover, the electrochemical surveys on these $Sm@C_{82}$ isomers reveal that their redox activities are mainly determined by the properties of their carbon cages.

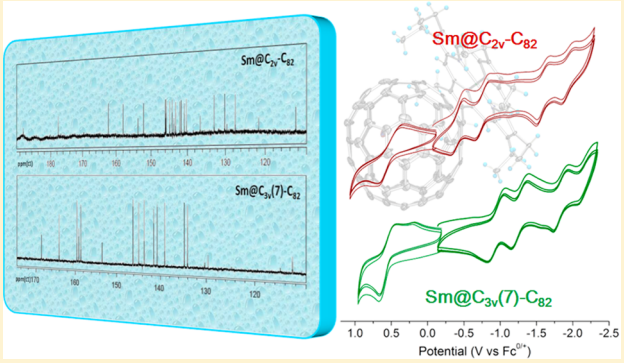

INTRODUCTION

Filling a fullerene cage with metals or a metallic cluster gives rise to the formation of endohedral metallofullerene (EMF). Such a concept has been developed a lot since the middle of 1990s, when an EMF (i.e., $La@C_{82}$) was detected and simply characterized for the first time by means of laser fragmentation.[1] In the past decade, a variety of EMFs have been synthesized, isolated, and characterized.[2,3] Great interest has been devoted to their unique structures and favorable properties. Particularly, $La@C_{82}$ and its analogous $M@C_{82}$ (M = group 2−3 elements and most lanthanides), which are more abundantly produced relative to others, have been widely studied and exhibited potential applications in the fields of medicine and material science.[4,5]

In contrast to the early discovery of $La@C_{82}$, its structure has remained unknown for a long time. The breakthrough was made by Nagase et al. in 1998.[6] They predicted the major isomer of $La@C_{2v}(9)$-C_{82} as well as the minor isomers of $La@C_s(6)$-C_{82} and $La@C_{3v}(7)$-C_{82} via theoretical calculations.[6] These predictions have been unambiguously confirmed by a number of subsequent studies of NMR and single crystal X-ray diffraction (XRD).[7−9] The electronic structures of these isomeric $La@C_{82}$ have been generally described using an electronic model of $La^{3+}@(C_{82})^{3-}$,[6] suggesting a formal transfer of three electrons between the metal and cage. It was believed that such a metal-cage interaction can contribute to the stabilization of the isomeric C_{82} cages.

Furthermore, recent studies revealed that these isomeric C_{82} cages can be stabilized not only by a trivalent metal ion but also by a divalent metal ion such as Ca^{2+}, Tm^{2+}, Yb^{2+}, and Sm^{2+}. The structures of divalent $M@C_{82}$ (M = Ca, Tm, Yb) have been characterized using XRD, NMR, and DFT calculations or a combination. Previous studies reported three isomers for $Tm@C_{82}$[10] and $Yb@C_{82}$[11] (i.e., $C_{2v}(9)$, $C_2(5)$, and $C_s(6)$ isomers) and four isomers for $Ca@C_{82}$[12] (i.e., $C_{2v}(9)$, $C_2(5)$, $C_s(6)$, and $C_{3v}(7)$ isomers). Among them, the $C_{3v}(7)$ isomer of $Ca@C_{82}$ was tentatively proposed based on an incomplete ^{13}C NMR spectrum, and the $C_{3v}(8)$ isomer could not be fully excluded. On the other hand, another divalent EMF $Sm@C_{82}$ has been studied by three independent groups. It is noteworthy that different metal sources were used by these groups, and they reported different isomeric distributions of $Sm@C_{82}$. Specifically, three isomers were obtained by using Sm_2O_3 as a samarium source, while four isomers were obtained by using $SmNi_2/Sm_2Co_{17}$ alloy as a metal source.[13,14] The three isomers reported by Liu et al. were characterized as $Sm@C_2(5)$-C_{82}, $Sm@C_s(6)$-C_{82}, and $Sm@C_{3v}(7)$-C_{82} using single crystal

Received: September 9, 2014
Published: February 13, 2015

DOI: 10.1021/ic5021884
Inorg. Chem. 2015, 54, 2103−2108

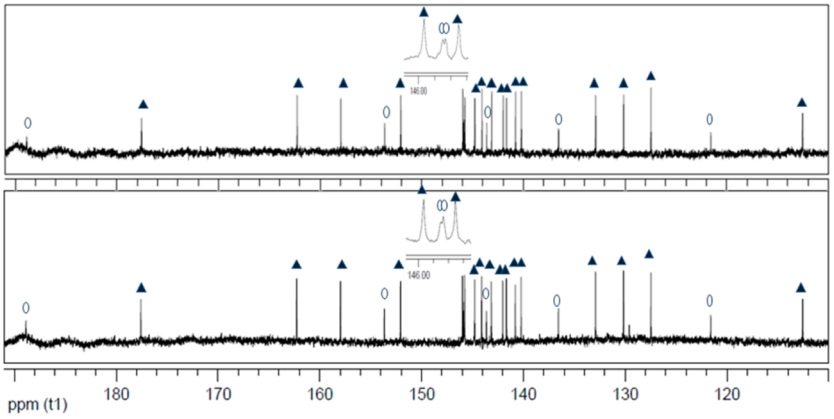

Figure 1. ^{13}C NMR spectra (125 MHz, in CS_2 using acetone-d_6 as internal lock, 293 K) of Sm@$C_{2v}(9)$-C_{82} in proton-coupled (up) and proton decoupled modes (down). The integrated intensity ratio of the peaks marked with a solid triangle and an open circle, respectively, is 2:1. Insets show the signals in the range of 145.5−146.2 ppm.

XRD,[13] while the fourth isomer reported by Shi et al. was proposed as Sm@$C_{2v}(9)$-C_{82} based on its UV−vis−NIR spectral characteristics.[14b] However, this proposal has never been confirmed by NMR or single crystal XRD. Herein, we demonstrate a full structural characterization of Sm@$C_{2v}(9)$-C_{82} as well as a complete NMR study of Sm@$C_{3v}(7)$-C_{82}, which might be valuable for the understanding of Sm@C_{82}. Moreover, the electrochemical surveys on these Sm@C_{82} isomers were performed to reveal their cage-dependent redox properties.

RESULTS AND DISCUSSION

Two Sm@C_{82} isomers were prepared and isolated according to the previously reported procedure and characterized by MALDI-TOF mass and UV−vis−NIR spectroscopy (see Figures S1, S2).[14a] One isomer was determined as Sm@$C_{2v}(9)$-C_{82} using a combined study of NMR and single crystal XRD. As shown in the proton decoupled or proton coupled ^{13}C NMR spectrum (see Figure 1), 24 signals (17 with full intensity and seven with half) are clearly seen in the range of 190−110 ppm at 293 K. This pattern evidently corresponds to the $C_{2v}(9)$-C_{82} cage, which corroborates well with the previous assignment based on the UV−vis−NIR spectroscopic studies.[14a] Moreover, summarizing all the previously reported ^{13}C NMR spectra of M@$C_{2v}(9)$-C_{82} (i.e., [La@$C_{2v}(9)$-C_{82}]$^-$, [Y@$C_{2v}(9)$-C_{82}]$^-$, [Pr@$C_{2v}(9)$-C_{82}]$^-$, and Yb@$C_{2v}(9)$-C_{82}), the ^{13}C signals of cage carbons are generally distributed in a narrow range (160−130 ppm) compared to those of Sm@$C_{2v}(9)$-C_{82}. It is noteworthy that there is no unpaired electron on the endohedral La^{3+}, Y^{3+}, Pr^{3+}, or Yb^{2+} ion, whereas Sm^{2+} has a $4f^6$ electronic structure, and thus, there are six unpaired f electrons on the endohedral Sm^{2+} ion. These unpaired electrons significantly affect the local magnetic field and the fast relaxation of ^{13}C nuclear spins on the adjacent cage carbons, thus contributing to the NMR chemical shifts of these cage carbons.

Furthermore, the absolute structure of Sm@$C_{2v}(9)$-C_{82} was determined via a single-crystal XRD study. A cocrystal of Sm@$C_{2v}(9)$-C_{82}/Ni^{II}(OEP) suitable for X-ray analysis was obtained by slow diffusion of a benzene solution of EMF into a $CHCl_3$ solution of Ni^{II}(OEP). The molecular structure was resolved and refined in a $C2/m$ (No. 12) space group.[15] Both the cage and endohedral metal atom were found to be disordered. In particular, two cage orientations with fractional occupancies of 0.27 and 0.23, respectively, have been identified. Figure 2 shows

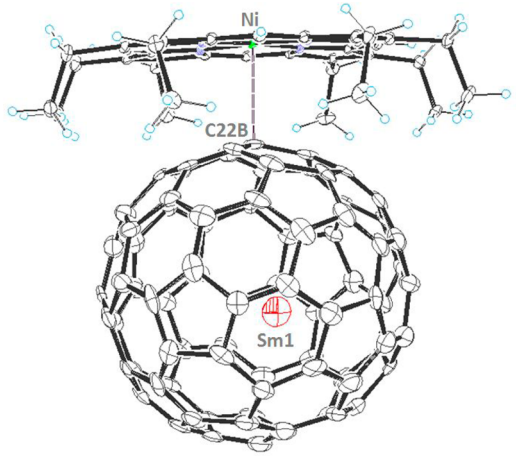

Figure 2. Ortep drawing of Sm@$C_{2v}(9)$-C_{82}·Ni^{II}(OEP) with 25% thermal ellipsoids, showing the relationship between the fullerene cage and Ni^{II}(OEP). Only the major cage orientation with 0.27 occupancy and the major Sm site (Sm1) with 0.118 occupancy are shown. The solvent molecules, other cage orientation, and metal ion sites are omitted for clarity.

the major cage orientation, the major samarium site (Sm1, 0.116 occupancy), and their relationships to Ni^{II}(OEP) moiety. The shortest C−Ni distance between a carbon ion of the major cage (C22B) and the Ni ion in Ni^{II}(OEP) was determined as 2.751(10) Å. This value is similar to those of 2.79(3) Å found in Yb@$C_{2v}(9)$-C_{82}·Ni^{II}(OEP), 2.78(2) Å in La@$C_{2v}(9)$-C_{82}·Ni^{II}(OEP), and 2.784(8) Å in Gd@$C_{2v}(9)$-C_{82}·Ni^{II}(OEP), reflecting the similar interactions between trivalent or divalent M@$C_{2v}(9)$-C_{82} and the Ni^{II}(OEP) moiety.

Inside the cage of $C_{2v}(9)$-C_{82}, multiple Sm sites were detected. Particularly, three sites (Sm4, Sm5, Sm6) reside on the crystallographic mirror plane, and other sites (Sm1, Sm2, Sm3, Sm7) are on general positions. Among them, Sm1 site has the highest occupancy, while other sites have occupancies ranging from 0.104 to 0.033. Moreover, additional Sm sites (Sm1A, Sm2A, Sm3A, Sm7A) are generated via the crystallographic mirror plane. Thus, there are totally 11 Sm sites inside the disordered $C_{2v}(9)$-C_{82} cages. Figure 3 shows the major cage orientation with all these metal sites. Because of the inherent disordered positions of the metal ions combined with a crystallographic mirror plane being mismatched with the

DOI: 10.1021/ic5021884
Inorg. Chem. 2015, 54, 2103−2108

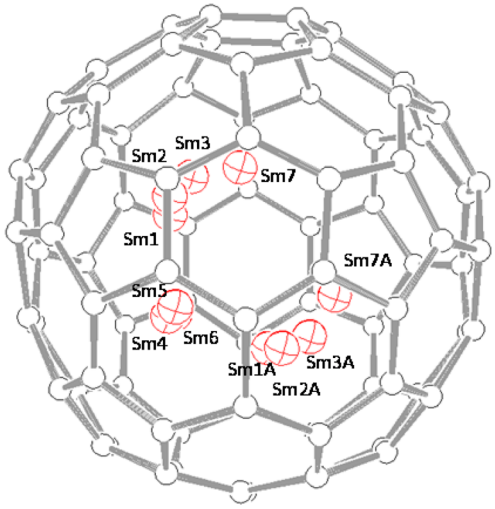

Figure 3. Diagram showing all the samarium sites inside the major cage of $C_{2v}(9)$-C_{82}. The sites Sm1−3A and Sm7A are generated from the sites Sm1−3 and Sm7 via the crystallographic mirror plane. Occupancies of these Sm sites are the following: Sm1, 0.116(3); Sm2, 0.104(3); Sm3, 0.083(4); Sm4, 0.066(4); Sm5, 0.051(6); Sm6, 0.033(5); and Sm7, 0.047(2). The sum of the occupancies of samarium sites Sm1−7 is 0.5, equal to the cage occupancy of 0.5.

molecular symmetry, the crystallographic data alone cannot determine the assignment of these Sm sites to each cage orientation. Nevertheless, theoretical calculations might provide more useful information. The previously calculated electrostatic potential map of $[C_{2v}(9)$-$C_{82}]^{2-}$ has demonstrated that the potential minimum is under a hexagon along the C_2 axis of the $C_{2v}(9)$-C_{82} cage, which usually corresponds to the position of endohedral divalent metal ion[11b,c] (see Figure S3). When considering the major cage orientation of $C_{2v}(9)$-C_{82}, metal sites Sm1−3 and Sm7 are found to be located close to or around the calculated potential minimum, indicating that these sites might be related to the major cage. Among them, the minor site Sm7 resides more closely to the potential minimum as compared to Sm1 and other Sm sites (see Figures S3, S4 for a detailed description). Therefore, DFT optimizations of Sm@$C_{2v}(9)$-C_{82} were performed at the M06-2*X*/3-21G ∼ SDD level starting from the models with Sm1 and Sm7 sites, respectively, both of which pointed to a structure as shown in Figure S5. It can be concluded that in the optimized Sm@$C_{2v}(9)$-C_{82} the Sm^{2+} ion is located slightly off the C_2 cage axis with a Sm-hexagon distance of 2.237 Å. It is noteworthy that the optimized Sm^{2+} position is different from the Sm1 site but very close to the Sm7 site as well as the Yb^{2+} position in the optimized Yb@$C_{2v}(9)$-C_{82}.[11b] The arrangement with the Sm^{2+} ion right along the C_2 axis is higher in energy by 0.732 kcal/mol with respect to the optimized Sm@$C_{2v}(9)$-C_{82}. Interestingly, the M06-2*X*/6-31G* ∼ SDD single-point calculations in the observed Sm@$C_{2v}(9)$-C_{82}/Ni^{II}(OEP) geometries (i.e., without any geometry optimizations, see Figure S4) place the moiety with the Sm7 site by 18.15 kcal/mol higher than the Sm1 species. To this end, despite the occupancy mismatch, it can be seen that the theoretical result, to some extent, agrees with the X-ray result. Therefore, the combined study of X-ray analysis and theoretical calculations might suggest that the preferred position of the Sm^{2+} ion in Sm@$C_{2v}(9)$-C_{82} is located slightly off the C_2 axis of $C_{2v}(9)$-C_{82}. Incidentally, the computed Mulliken charge on Sm is +1.955*e*, confirming the electronic structure of Sm^{2+}@$[C_{2v}(9)$-$C_{82}]^{2-}$.

As for another Sm@C_{82} isomer, both the proton decoupled and proton coupled ^{13}C NMR spectra are shown in Figure 4. Each spectrum displays 16 signals (12 with full intensity, three with half and one with 1/6) in the range of 170−110 ppm at 293 K. This pattern can be unambiguously assigned to the cage of $C_{3v}(7)$-C_{82} rather than $C_{3v}(8)$-C_{82}. Such a result is consistent with the assignment based on the UV−vis−NIR spectroscopic studies.[12] As compared with the previously reported NMR data of Ca@$C_{3v}(7)$-C_{82},[12a] which demonstrate signals in the range of 150−130 ppm, the wider signal distribution of Sm@$C_{3v}(7)$-C_{82} again indicates the paramagnetic effect of the endohedral Sm^{2+} ion. Moreover, because there is only one ^{13}C NMR signal having 1/6 intensity in the spectrum, it can be safely assigned to the carbon C(82) (see Figure S6) that is the only carbon residing along the C_3 axis of the $C_{3v}(7)$-C_{82} cage. Note that this carbon has a lower chemical shift (i.e., 114.96 ppm) relative to most others in the spectrum, indicating a significant paramagnetic effect imposed by the closely located paramagnetic Sm^{2+} ion. A similar situation was also observed in the ^{13}C NMR spectrum of $[$Ce@$C_{2v}(9)$-$C_{82}]^{-}$, in which the signals with lower chemical shifts were assigned to the hexagon that is along the C_2 axis and close to the paramagnetic Ce^{3+} ion. Therefore, the NMR study of Sm@$C_{3v}(7)$-C_{82} might indicate that the internal

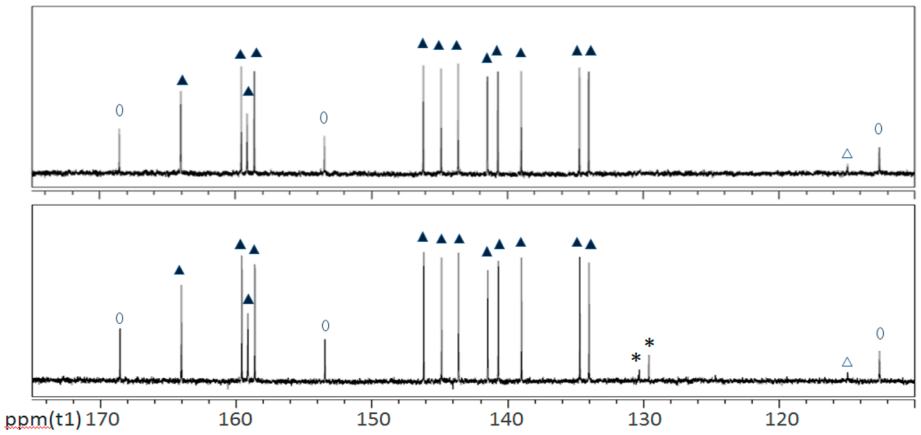

Figure 4. ^{13}C NMR spectra (125 MHz, in CS_2 using acetone-d_6 as internal lock, 293 K) of Sm@$C_{3v}(7)$-C_{82} in proton-coupled (up) and proton decoupled modes (down). The integrated intensity ratio of the peaks marked with a solid triangle, an open circle, and an open triangle, respectively, is 6:3:1. The asterisk (*) indicates the signals from impurities.

DOI: 10.1021/ic5021884
Inorg. Chem. 2015, 54, 2103−2108

Table 1. Redox Potentials (V vs $Fc^{0/+}$)[a] of $Sm@C_{2v}(9)$-C_{82}, $Sm@C_{3v}(7)$-C_{82}, and Reference Fullerenes

	$^{ox}E_1$	$^{red}E_1$	$^{red}E_2$	$^{red}E_3$	$^{red}E_4$	$\triangle E_{gap,EC}$	abs. onset
$Sm@C_{2v}(9)$-C_{82}	0.52	−0.42	−0.77	−1.60	−1.94	0.94	1766 (0.70)[f]
$Yb@C_{2v}(9)$-C_{82}[d]	0.61	−0.46	−0.78	−1.60	−1.90	1.07	
$Sm@C_2(5)$-C_{82}[e]	0.42	−0.84	−1.01	−1.51	−1.90	1.26	1402 (0.88)[f,g]
$Yb@C_2(5)$-C_{82}[d]	0.38	−0.86	−0.98	−1.50	−1.87	1.24	
$Sm@C_{3v}(7)$-C_{82}	0.66[b](0.56[c])	−0.94	−1.25	−1.79	−2.11	1.50	1128 (1.10)[f]

[a]Half-wave potentials unless otherwise noted. [b]Irreversible process; peak potential. [c]DPV value. [d]Ref 11a. [e]Ref 16. [f]Absorption onset position; units: nm (eV). [g]Values reported by ref 13.

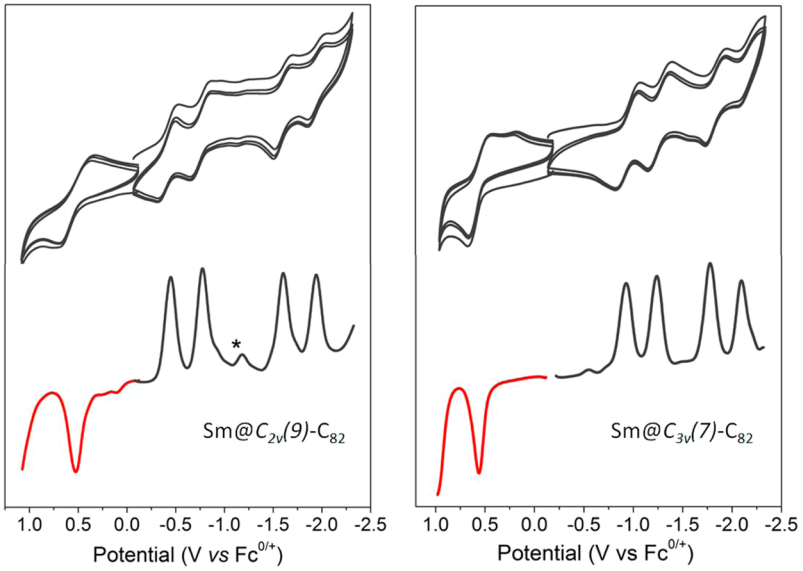

Figure 5. Cyclic voltammograms and differential pulse voltammogram of $Sm@C_{2v}(9)$-C_{82} (left) and $Sm@C_{3v}(7)$-C_{82} (right) in o-dichlorobenzene containing 0.05 M $(n\text{-Bu})_4NPF_6$, (scan rate: 100 mV s^{-1} and 20 mV s^{-1} for CV and DPV, respectively). The asterisk (*) corresponds to the trace impurities in the sample or solvent.

Sm^{2+} ion prefers to reside along the C_3 axis and very close to the carbon C(82). Such a proposal agrees very well with the previously reported XRD data, which demonstrated a similar Sm^{2+} ion position as well as a close metal-cage contact between Sm and C(82) in $Sm@C_{3v}(7)$-C_{82}.[13]

Electrochemical surveys of $Sm@C_{2v}(9)$-C_{82} and $Sm@C_{3v}(7)$-C_{82} were performed by means of cyclic voltammogram (CV) and differential pulse voltammogram (DPV). CV and DPV were recorded in *o*-dichlorobenzene (*o*-DCB) containing 0.05 M tetra-(*n*-butyl)-ammonium hexafluoro-phosphate ($(n\text{-Bu})_4NPF_6$) as a supporting electrolyte. All the obtained redox potentials were summarized in Table 1 and compared with those of previously reported $Sm@C_2(5)$-C_{82}.[16] As shown in the CV profiles (see Figure 5), these $Sm@C_{82}$ isomers all exhibit four reversible one-electron reduction steps in the cathodic region, while the difference of their first or second reduction potentials exceeds 0.5 V. Specifically, the first reduction potential of $Sm@C_{3v}(7)$-C_{82} is much higher than those of other two isomers, shifting from −0.94 V for $Sm@C_{3v}(7)$-C_{82} to −0.84 V for $Sm@C_2(5)$-C_{82} and −0.42 V for $Sm@C_{2v}(9)$-C_{82}. Apparently, the reduction potentials of these $Sm@C_{82}$ isomers are mainly determined by the properties of their carbon cages, and $Sm@C_{3v}(7)$-C_{82} exhibits a much weaker electron-accepting ability relative to others. As for the third or fourth reductions, the potential difference between these isomers is almost negligible. Such a feature suggests that the LUMO+1 orbitals of $Sm@C_{82}$ isomers are less susceptible to the cage symmetries as compared to their nondegenerate low-lying LUMOs. On the other hand, in the anodic region, the CV of $Sm@C_{3v}(7)$-C_{82} at a scan rate of 100 mV s^{-1} shows an irreversible one-electron oxidation step with a peak potential at 0.66 V. Decreasing the scan rate from 100 mV s^{-1} to 50 mV s^{-1}, the first oxidation of $Sm@C_{3v}(7)$-C_{82} becomes even more irreversible (see Figure S7). The other two isomers both exhibit fully reversible oxidations at 0.52 and 0.42 V ($E_{1/2}$ vs Fc/Fc^+), respectively. Thus, the oxidative behaviors of $Sm@C_{82}$ isomers are cage-dependent. All these redox steps can also be observed in the corresponding DPV profiles. The electrochemical gap was determined as 1.5 eV for $Sm@C_{3v}(7)$-C_{82},[17] 0.94 eV for $Sm@C_{2v}(9)$-C_{82}, and 1.26 eV for $Sm@C_2(5)$-C_{82}, respectively, which are consistent with the magnitude of their absorption onset positions (see Table 1). Moreover, another comparison study demonstrated an unremarkable potential difference (less than 90 mV) between $Sm@C_{2v}(9)$-C_{82} and $Yb@C_{2v}(9)$-C_{82}. Also, the potential difference between $Sm@C_2(5)$-C_{82} and $Yb@C_2(5)$-C_{82} is even smaller than 40 mV.[15] These results suggest that replacing the endohedral Yb^{2+} ion with the Sm^{2+} ion does not significantly influence the redox properties of $M@C_{82}$.

CONCLUSIONS

In conclusion, two $Sm@C_{82}$ isomers have been structurally characterized by ^{13}C NMR spectroscopy for the first time, and their cage symmetries were unambiguously determined as $C_{2v}(9)$ and $C_{3v}(7)$, respectively. A combined study of single crystal X-ray analysis and theoretical calculations suggest that the preferred Sm^{2+} ion position in $Sm@C_{2v}(9)$-C_{82} might be

DOI: 10.1021/ic5021884
Inorg. Chem. 2015, 54, 2103−2108

located in a region slightly off the C_2 axis of $C_{2v}(9)$-C_{82}. Moreover, the electrochemical surveys on these Sm@C_{82} isomers reveal that their redox activities are mainly determined by the properties of their carbon cages. Therefore, our results not only further complete the knowledge of divalent M@C_{82} but also enhance the understanding of the structures and electrochemical properties of these Sm@C_{82} isomers.

EXPERIMENTAL SECTION

Synthesis and Isolation. The synthesis of Sm-metallofullerenes was described in earlier studies.[14] Briefly, Sm-metallofullerenes were produced using a modified arc-discharge method. Specifically, the anode graphite rod was filled with $SmNi_2$/graphite powder (1:10 atomic ratio), while a pure graphite rod was employed as a cathode. The arc-discharge was carried out at 70 A with an electrode gap of ca. 1 cm under 400 Torr helium static atmosphere. Fullerene species was extracted from soot using *o*-xylene at a high temperature under a nitrogen atmosphere. The pure samples of Sm@$C_{2v}(9)$-C_{82} and Sm@$C_{3v}(7)$-C_{82} were isolated via a multistage HPLC procedure and then checked by analysis HPLC.

NMR Experiments. The ^{13}C NMR measurements were conducted with a spectrometer (Avance 500 with a Cryo-Probe system; Bruker) in proton-decoupled and proton-coupled modes, respectively. Carbon disulfide was used as a solvent and a capillary tube of acetone-d_6 as an internal lock. ^{13}C NMR (125 MHz, CS_2, 293 K) of Sm@$C_{2v}(9)$-C_{82}: δ 188.87(2C), 177.56(4C), 162.26(4C), 157.96(4C), 153.65(2C), 152.06(4C), 145.97(4C), 145.85(2C), 145.83(2C), 145.75(4C), 144.78(4C), 144.08(4C), 143.61(2C), 143.13(4C), 142.00(4C), 141.65(4C), 140.78(4C), 140.21(4C), 136.55(2C), 132.90(4C), 130.15(4C), 127.46(4C), 121.58(2C), 112.54(4C) ppm. ^{13}C NMR (125 MHz, CS_2, 293 K) of Sm@$C_{3v}(7)$-C_{82}: δ 168.55(3C), 164.03(6C), 159.58(6C), 159.14(6C), 158.61(6C), 153.46(3C), 146.17(6C), 144.87(6C), 143.62(6C), 141.46(6C), 140.69(6C), 138.98(6C), 134.68(6C), 134.01(6C), 114.96(1C), 112.62(3C) ppm.

Single-crystal X-ray Diffraction Analysis. Black cocrystals of Sm@$C_{2v}(9)$-C_{82}/Ni^{II}(OEP) were obtained by allowing the benzene solution of fullerene and the chloroform solution of Ni^{II}(OEP) to diffuse together. X-ray data were collected at 90 K using a diffractometer (APEX II; Bruker Analytik GmbH) equipped with a CCD collector. The multiscan method was used for absorption correction. The structure was resolved using direct methods (SHELXS97) and refined on F^2 using full-matrix least-squares using SHELXL97.[18] The intact cage was modeled via the crystallographic mirror plane in refinement. The sum of the occupancy factors for all samarium sites was set as 0.5, equal to the sum of cage occupancy of 0.5. Hydrogen atoms were added geometrically and refined with a riding model.

The cocrystal of Sm@$C_{2v}(9)$-C_{82}·Ni^{II}(OEP)·0.87C_6H_6·0.13$CHCl_3$ contains another severely disordered lattice of C_6H_6 and $CHCl_3$ molecules that could not be modeled properly. Therefore, the SQUEEZE program, a part of the PLATON package of crystallographic software,[19] was used to calculate the solvent disorder area and remove its contribution from the intensity data.

Electrochemistry. Differential pulse voltammetry (DPV) and cyclic voltammetry (CV) were carried out in *o*-dichlorobenzene (*o*-DCB) using a BAS CW-50 instrument. A conventional three-electrode cell consisting of a platinum working electrode, a platinum counter-electrode, and a saturated calomel reference electrode (SCE) was used for both measurements. 0.05 M $(n\text{-}Bu)_4NPF_6$ was used as the supporting electrolyte. All potentials were recorded against a SCE reference electrode and corrected against Fc/Fc^+. DPV and CV were measured at a scan rate of 20 and 100 mVs^{-1}, respectively.

COMPUTATIONAL METHOD

Single point calculations and geometry optimizations were carried out using the Gaussian 09 program package[20] at the M06-2X/3-21G(6-31G*) ~ SDD level.[21] The standard 3-21G or 6-31G* basis set was used for the C, N, and H atoms and the SDD basis set (with the SDD effective core potential) for Sm and Ni atoms.

ASSOCIATED CONTENT

Supporting Information

Mass and UV−vis−NIR spectra of Sm@$C_{2v}(9)$-C_{82} and Sm@$C_{3v}(7)$-C_{82}, X-ray models of Sm@$C_{2v}(9)$-C_{82}, CV profiles of Sm@$C_{3v}(7)$-C_{82}, X-ray crystallographic file in CIF format for Sm@C_{2v}-C_{82}·Ni^{II}(OEP)·0.87C_6H_6·0.13$CHCl_3$, and complete ref 20. This material is available free of charge via the Internet at http://pubs.acs.org.

AUTHOR INFORMATION

Corresponding Authors

*E-mail: zjshi@pku.edu.cn.
*E-mail: fenglai@suda.edu.cn.

Notes

The authors declare no competing financial interest.

ACKNOWLEDGMENTS

This work is supported in part by NSF of China (21171013, 51372158, 21471010), the Ministry of Science and Technology of China (No. 2013CB933402, No. 2011CB932601), Jiangsu Specially Appointed Professor Program (SR10800113), the Project for Jiangsu Scientific and Technological Innovation Team (2013), and the Czech Science Foundation/GACR (P208/10/1724). Also, we are grateful to prof. T. Akasaka at the University of Tsukuba for his kind support in NMR and XRD measurements.

REFERENCES

(1) Lorents, D. C.; Yu, D. H.; Brink, C.; Jensen, N.; Hvelplund, P. *Chem. Phys. Lett.* **1995**, *236*, 141.

(2) (a) Akasaka, T.; Nagase, S. *Endofullerenes: A New Family of Carbon Clusters*; Kluwer: Dordrecht, The Netherlands, 2002. (b) Shinohara, H. *Rep. Prog. Phys.* **2000**, *63*, 843. (c) Feng, L.; Akasaka, T.; Nagase, S. In *Carbon Nanotubes and Related Structures*; Guldi, D. M., Martin, N., Eds.; Wiley-VCH: Weinheim, 2010; p 455.

(3) (a) Chaur, M. N.; Melin, F.; Ortiz, A. L.; Echegoyen, L. *Angew. Chem., Int. Ed.* **2009**, *48*, 7514. (b) Lu, X.; Feng, L.; Akasaka, T.; Nagase, S. *Chem. Soc. Rev.* **2012**, *41*, 7723. (c) Zhang, J.; Stevenson, S.; Dorn, H. C. *Acc. Chem. Res.* **2013**, *46*, 1548. (d) Popov, A. A.; Yang, S.; Dunsch, L. *Chem. Rev.* **2013**, *113*, 5989. (e) Wang, T.; Wang, C. *Acc. Chem. Res.* **2014**, *47*, 450.

(4) (a) Fatouros, P. P.; Corwin, F. D.; Chen, Z. J.; Broaddus, W. C.; Tatum, J. L.; Kettenmann, B.; Ge, Z.; Gibson, H. W.; Russ, J. L.; Leonard, A. P.; Duchamp, J. C.; Dorn, H. C. *Radiology* **2006**, *240*, 756. (b) Bolskar, R. D. *Nanomedicine* **2008**, *3*, 201.

(5) (a) Sato, S.; Seki, S.; Honsho, Y.; Wang, L.; Nikawa, H.; Luo, G.; Lu, J.; Haranaka, M.; Tsuchiya, T.; Nagase, S.; Akasaka, T. *J. Am. Chem. Soc.* **2011**, *133*, 2766. (b) Sato, S.; Nikawa, H.; Seki, S.; Wang, L.; Luo, G. F.; Lu, J.; Haranaka, M.; Tsuchiya, T.; Nagase, S.; Akasaka, T. *Angew. Chem., Int. Ed.* **2012**, *51*, 1589. (c) Feng, L.; Rudolf, M.; Wolfrum, S.; Troeger, A.; Slanina, Z.; Akasaka, T.; Nagase, S.; Martín, N.; Ameri, T.; Brabec, C. J.; Guldi, D. M. *J. Am. Chem. Soc.* **2012**, *134*, 12190. (d) Rudolf, M.; Feng, L.; Slanina, Z.; Akasaka, T.; Nagase, S.; Guldi, D. M. *J. Am. Chem. Soc.* **2013**, *135*, 11165.

(6) (a) Kobayashi, K.; Nagase, S. *Chem. Phys. Lett.* **1998**, *282*, 325. (b) Lu, J.; Zhang, X. W.; Zhao, X. G.; Nagase, S.; Kobayashi, K. *Chem. Phys. Lett.* **2000**, *332*, 219.

(7) (a) Akasaka, T.; Wakahara, T.; Nagase, S.; Kobayashi, K.; Waelchli, M.; Yamamoto, K.; Kondo, M.; Shirakura, S.; Okubo, S.; Maeda, Y.; Kato, T.; Kako, M.; Nakadaira, Y.; Nagahata, R.; Gao, X.; Van Caemelbecke, E.; Kadish, K. M. *J. Am. Chem. Soc.* **2000**, *122*, 9316. (b) Maeda, Y.; Matsunaga, Y.; Wakahara, T.; Takahashi, S.; Tsuchiya, T.; Ishitsuka, M. O.; Hasegawa, T.; Akasaka, T.; Liu, M. T.

DOI: 10.1021/ic5021884
Inorg. Chem. 2015, 54, 2103−2108

H.; Kokura, K.; Horn, E.; Yoza, K.; Kato, T.; Okubo, S.; Kobayashi, K.; Nagase, S.; Yamamoto, K. *J. Am. Chem. Soc.* **2004**, *126*, 6858. (c) Feng, L.; Nakahodo, T.; Wakahara, T.; Tsuchiya, T.; Maeda, Y.; Akasaka, T.; Kato, T.; Horn, E.; Yoza, K.; Mizorogi, N.; Nagase, S. *J. Am. Chem. Soc.* **2005**, *127*, 17136.

(8) Akasaka, T.; Wakahara, T.; Nagase, S.; Kobayashi, K.; Waelchli, M.; Yamamoto, K.; Kondo, M.; Shirakura, S.; Maeda, Y.; Kato, T.; Kako, M.; Nakadaira, Y.; Gao, X.; Van Caemelbecke, E.; Kadish, K. M. *J. Phys. Chem. B* **2001**, *105*, 2971.

(9) Akasaka, T.; Lu, X.; Kuga, H.; Nikawa, H.; Mizorogi, N.; Slanina, Z.; Tsuchiya, T.; Yoza, K.; Nagase, S. *Angew. Chem., Int. Ed.* **2011**, *49*, 9715.

(10) Kodama, T.; Ozawa, N.; Miyake, Y.; Sakaguchi, K.; Nishikawa, H.; Ikemoto, I.; Kikuchi, K.; Achiba, Y. *J. Am. Chem. Soc.* **2002**, *124*, 1452.

(11) (a) Lu, X.; Slanina, Z.; Akasaka, T.; Tsuchiya, T.; Mizorogi, N.; Nagase, S. *J. Am. Chem. Soc.* **2010**, *132*, 5896. (b) Suzuki, M.; Slanina, Z.; Mizorogi, N.; Lu, X.; Nagase, S.; Olmstead, M. M.; Balch, A. L.; Akasaka, T. *J. Am. Chem. Soc.* **2012**, *134*, 18772. (c) Mizorogi, N.; Nagase, S. *Chem. Phys. Lett.* **2006**, *431*, 110.

(12) (a) Kodama, T.; Fujii, R.; Miyake, Y.; Sakaguchi, K.; Nishikawa, H.; Ikemoto, I.; Kikuchi, K.; Achiba, Y. *Chem. Phys. Lett.* **2003**, *377*, 197. (b) Xu, Z.; Nakane, T.; Shinohara, H. *J. Am. Chem. Soc.* **1996**, *118*, 11309.

(13) Yang, H.; Jin, H.; Wang, X.; Liu, Z.; Yu, M.; Zhao, F.; Mercado, B. Q.; Olmstead, M. M.; Balch, A. L. *J. Am. Chem. Soc.* **2012**, *134*, 14127.

(14) (a) Okazaki, T.; Lian, Y. F.; Gu, Z. N.; Suenaga, K.; Shinohara, H. *Chem. Phys. Lett.* **2000**, *320*, 435. (b) Liu, J.; Shi, Z. J.; Gu, Z. N. *Chem.—Asian J.* **2009**, *4*, 1703.

(15) Crystal data for Sm@$C_{2v}(9)$-C_{82}·Ni^{II}(OEP)·0.87C_6H_6·0.13$CHCl_3$: $C_{123.34}H_{49.34}Cl_{0.40}SmN_4Ni$, Mr = 1810.69, 0.28 × 0.15 × 0.12 mm, monoclinic, $C2/m$ (no. 12), a = 25.3280(18), b = 15.1696(11), c = 19.7982(14), β = 95.052(1)°, V = 7577.2(9) Å^3, Z = 4, ρ_{calc} = 1.587 g cm^{-3}, μ (Mo Kα) = 1.097 mm^{-1}, θ = 4.26−29.57°, T = 90 K, R_1 = 0.1278, wR_2 = 0.3966 for all data; R_1 = 0.1177, wR_2 = 0.3804 for 10 957 reflections ($I > 2.0\sigma(I)$) with 1283 parameters. Maximum residual electron density 1.951 e Å^{-3}.

(16) Xu, W.; Niu, B.; Feng, L.; Shi, Z.; Lian, Y. *Chem.—Eur. J.* **2012**, *18*, 14246.

(17) Calculated from DPV values.

(18) Sheldrick, G. *Acta Crystallogr., Sect. A* **2008**, *64*, 112.

(19) (a) Spek, A. L. *PLATON. A multipurpose crystallographic tool*; Utrecht University: The Netherlands, 2003. (b) SQUEEZE: van der Sluis, P.; Spek, A. L. *Acta Crystallogr., Sect. A* **1990**, *46*, 194.

(20) Frisch, M. J. et al. *Gaussian 09*, revision A.02, Gaussian, Inc.: Wallingford, CT, 2009.

(21) (a) Zhao, Y.; Truhlar, D. *Theor. Chem. Acc.* **2008**, *120*, 215. (b) Becke, A. D. *J. Chem. Phys.* **1993**, *98*, 5648. (c) Cao, X.; Dolg, M. *THEOCHEM* **2002**, *581*, 139.

DOI: 10.1021/ic5021884
Inorg. Chem. 2015, 54, 2103−2108